

Graphene-Enabled Silver Nanoantenna Sensors

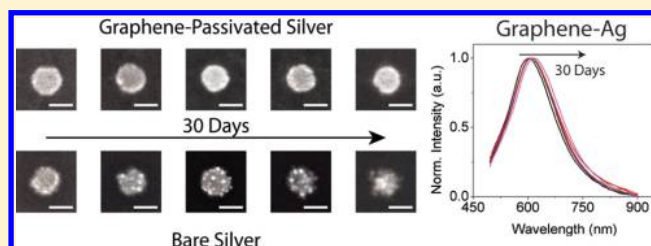
Jason C Reed, Hai Zhu, Alexander Y. Zhu, Chen Li, and Ertugrul Cubukcu*

Department of Materials Science and Engineering, University of Pennsylvania, Philadelphia, Pennsylvania 19104, United States

Supporting Information

ABSTRACT: Silver is the ideal material for plasmonics because of its low loss at optical frequencies but is often replaced by a more lossy metal, gold. This is because of silver's tendency to tarnish and roughen, forming Ag_2S on its surface, dramatically diminishing optical properties and rendering it unreliable for applications. By passivating the surface of silver nanostructures with monolayer graphene, atmospheric sulfur containing compounds are unable to penetrate the graphene to degrade the surface of the silver. Preventing this sulfidation eliminates the increased material damping and scattering losses originating from the unintentional Ag_2S layer. Because it is atomically thin, graphene does not interfere with the ability of localized surface plasmons to interact with the environment in sensing applications. Furthermore, after 30 days graphene-passivated silver (Ag-Gr) nanoantennas exhibit a 2600% higher sensitivity over that of bare Ag nanoantennas and 2 orders of magnitude improvement in peak width endurance. By employing graphene in this manner, the excellent optical properties and large spectral range of silver can be functionally utilized in a variety of nanoscale plasmonic devices and applications.

KEYWORDS: Plasmonics, graphene, LSPR sensor, nanoantennas, silver, sulfidation



Many have studied and continue to study the optical properties of metallic nanoparticles for the collective light-matter interaction phenomenon known as localized surface plasmon resonance (LSPR).^{1,2} Because of intense local electric field enhancements and sharp resonant extinction peaks, metallic nanoparticles are of great interest for bio/molecular sensors and nonlinear optical studies, as well as surface-enhanced Raman spectroscopy.³⁻⁷ In the visible regime, silver is the ideal plasmonic metal with lower losses and a higher operation frequency, due to the lack of interband absorption than that of either gold or copper.⁸ However, when exposed to ambient air, trace amounts of atmospheric hydrogen sulfide (H_2S) and carbonyl sulfide (OCS) readily react with the surface of the silver, forming Ag_2S .⁹⁻¹² Not only does the sulfidation increase the material loss in the plasmonic nanoantennas, changes to the surface morphology lead to increased surface scattering loss as well.^{13,14}

Because of the chemical instability of silver, gold is often used instead despite having inferior plasmonic properties. While there have been efforts to encapsulate and passivate Ag surfaces to retain its excellent properties, the encapsulating layer is often as thick as or thicker than the nanostructures themselves.^{15,16} This poses a problem for LSPR sensing, as it relies on near-field interactions which are the strongest on the surface of the particle.¹⁷ Among its many excellent properties enabling myriad different applications,¹⁸⁻²² atomically thin graphene has been proven to be impenetrable to gas molecules as small as helium atoms.^{23,24} Thus, passivating the surface of plasmonic silver nanoparticles (or nanoantennas) with monolayer graphene could prevent the reaction of the silver surface with sulfur compounds, preserving not only its excellent plasmonic

properties but also its LSPR sensing ability. The rising price of gold also needs to be considered for the commercialization of gold-based devices. Given the 58-times reduction in price of silver (July 2012) over that of gold and the advances in graphene synthesis, economics may drive the next generation of commercial plasmonic devices. Additionally, silver does not suffer from large losses at wavelengths shorter than 600 nm (in contrast to Au or Cu) and can be utilized over the entire visible range.⁸

To test the efficacy of graphene as an effective solution to the problem of silver sulfidation, silver nanoantennas were fabricated with a layer of graphene on top, as illustrated in Figure 1a. The Ag nanoantennas arrays were fabricated on cleaned glass substrates spin-casted with 50/50 nm of 950/495 K molecular weight bilayer poly(methyl methacrylate) (PMMA). A 5 nm layer of Cr was thermally deposited on top of the PMMA to act as a charge dissipation layer. The patterns were written using an Elionix ELS-7500EX e-beam writer. The $100 \times 100 \mu\text{m}^2$ areas were patterned with circles in a square array. The dimensions of the nanoantennas were 115 nm in diameter and 300 nm in interparticle spacing. After e-beam writing, the Cr layer was etched away using Transene Cr Etch 1020 and the samples developed in 1:3 methyl isobutyl ketone (MIBK)/isopropanol (IPA) for 60 s. After brief O_2 plasma cleaning, the samples were placed into an e-beam evaporator to deposit 3/30 nm of Ge/Ag. Acetone was used for metal liftoff with 10 s of sonication after a 30 min soak.

Received: April 25, 2012

Revised: July 11, 2012

Published: July 15, 2012

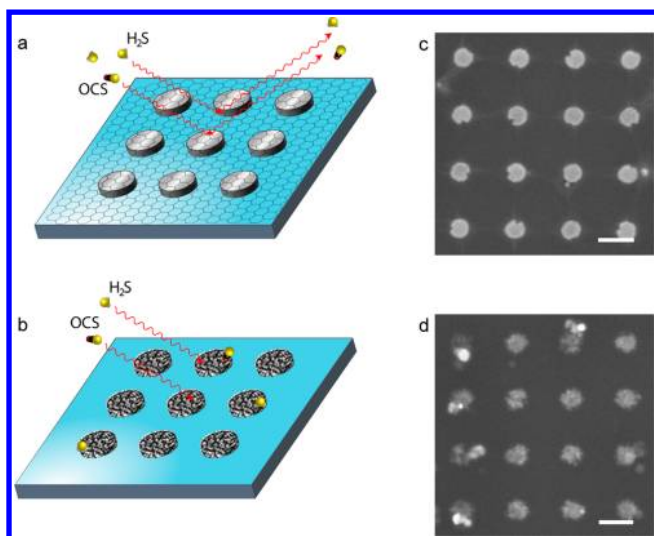


Figure 1. (a) Illustration of graphene-passivated Ag nanoantennas fabricated in a square array. The graphene layer prevents the reaction of trace atmospheric H_2S and OCS with the surface of the Ag. (b) Illustration of bare Ag nanoantennas fabricated similarly. The lack of graphene allows the atmospheric sulfur compounds to react with the silver. SEM images of (c) graphene-passivated Ag nanoantennas and (d) bare Ag nanoantennas after 30 days; scale bars are 200 nm.

Two silver nanoantenna arrays were identically fabricated. One of the nanoantenna arrays was covered with a layer of graphene, while the second was left as bare Ag (Figure 1b). To transfer the graphene, CVD-grown graphene on copper foil was used as purchased (Graphene Supermarket). Following the methods of Ruoff et al.,^{25,26} PMMA (350 K MW at 45 mg/mL in anisole) was spin-cast (4000 rpm, 45 s) onto the foil before etching the Cu foil with 1 M iron chloride solution for 45 min at 75 °C. The PMMA/graphene film was then transferred to deionized water and washed multiple times. The graphene layer was then transferred to the Ag nanoantennas sample immediately after Ag metal liftoff and allowed to dry in vacuum. After drying, a drop of the PMMA solution was added and allowed to recure for 30 min in air before washing multiple times in acetone/IPA. The total time in ambient air after Ag film deposition and graphene coverage was one hour. Sulfidation of nanoscale Ag can be as much as 3 nm/day,⁹ leading to, at most, a 1 Å layer of sulfide formation before graphene coverage. The two samples were then stored in ambient laboratory environment for 30 days. As shown in Figure 1c, the Ag nanoantennas covered by graphene did not show signs of sulfidation; the surfaces of the particles were smooth and kept their circular shape. Bare Ag nanoantennas, as seen in Figure 1d, show large morphological changes to the disks. The presence of sulfur on the surface of the unpassivated nanoparticles has also been confirmed through energy-dispersive X-ray spectroscopy (EDX) (Supporting Information, Figure S1). Bare Ag nanoantennas showed a sulfur peak in the EDX data, while graphene-passivated Ag nanoantennas lacked that peak in the spectrum.

The graphene passivation of the silver nanoantennas has a dramatic effect on its optical properties and morphology. The morphological changes that are prevented by the graphene passivation can be seen even within the same sample array. Particles covered by graphene show no signs of morphology changes, while those left uncovered by cracks in the graphene film show large changes in morphology (Supporting

Information, Figure S2). This is also true for continuous Ag films (Supporting Information, Figure S3), where a well-defined boundary of sulfidation and surface roughness change formed at the edge of the graphene layer.

The optical spectra of the nanoparticle arrays were measured over 30 days to study how well graphene passivation retained the properties of Ag. Reflection spectra of the nanoantennas were taken using a homemade free-space microscope. A fiber-coupled light source (Ocean Optics LS-1) was collimated using a lens before passing through a 50:50 beam splitter. The light passed through a 50× objective (Mitutoyo, 0.42 NA) and focused onto the surface of the sample. The reflected light passed back through the objective and beam splitter and was imaged by a tube lens (Mitutoyo) and focused by a 10× objective (Olympus, 0.25 NA) into a fiber-coupled CCD spectrometer (Thor Laboratories CCS175). All measurements were normalized to the substrate without nanoantennas and sampled using 50 ms exposure time, 50× spectrum averaging, and 50× boxcar averaging. Figure 2a shows the temporal

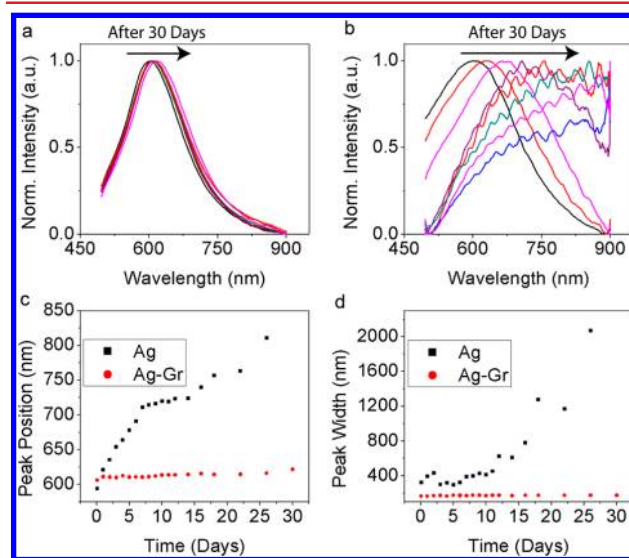


Figure 2. Normalized reflection spectra of (a) graphene-passivated Ag and (b) bare Ag nanoantennas over the course of 30 days. Time evolution of the (c) resonance peak position and the (d) resonance peak width for both graphene-passivated and bare Ag nanoantennas over 30 days.

evolution of the spectrum for graphene-passivated Ag nanoantennas, while Figure 2b shows that of as-fabricated Ag nanoantennas. Over a 30 day period, both the resonant peak position, λ_{max} (Figure 2c), as well as the resonant peak width, $\Delta\lambda$ (Figure 2d), increased dramatically for unpassivated Ag nanoantennas. In contrast, the Ag nanoantennas that were passivated by the graphene showed a much more robust preservation of the initial plasmonic properties. The shift in λ_{max} for the unpassivated Ag nanoantennas was 216 nm compared to 15 nm for that of graphene-passivated Ag nanoantennas. The increase in the peak width for bare Ag nanoantennas was 1748 nm, while only 11 nm for that of passivated Ag nanoantennas.

The usefulness of plasmonic resonances for sensing applications depends highly upon the peak width. The graphene-passivated Ag nanoantennas show about a 160 fold resistance to peak width increases over the 30 day period. Additionally, the sensitivity to small shifts in the spectrum can be quantified by the slope of the resonant spectra ($dI/d\lambda$).

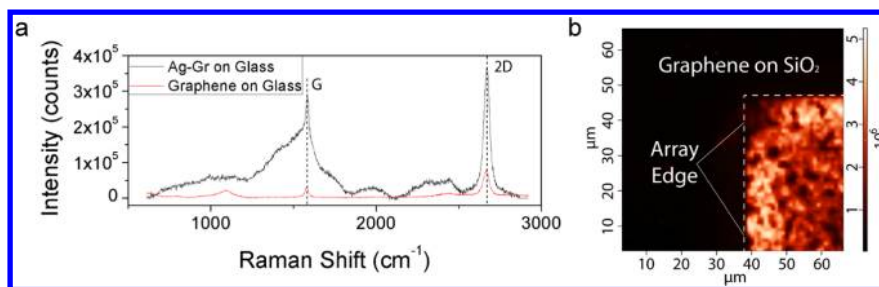


Figure 3. (a) Raman spectra of graphene both on and off of the Ag nanoantenna array, with the relative intensities of the G and 2D bands suggesting monolayer graphene. (b) Raman intensity map of the 2D band on the corner of the Ag nanoantenna array, showing the relative enhancement.

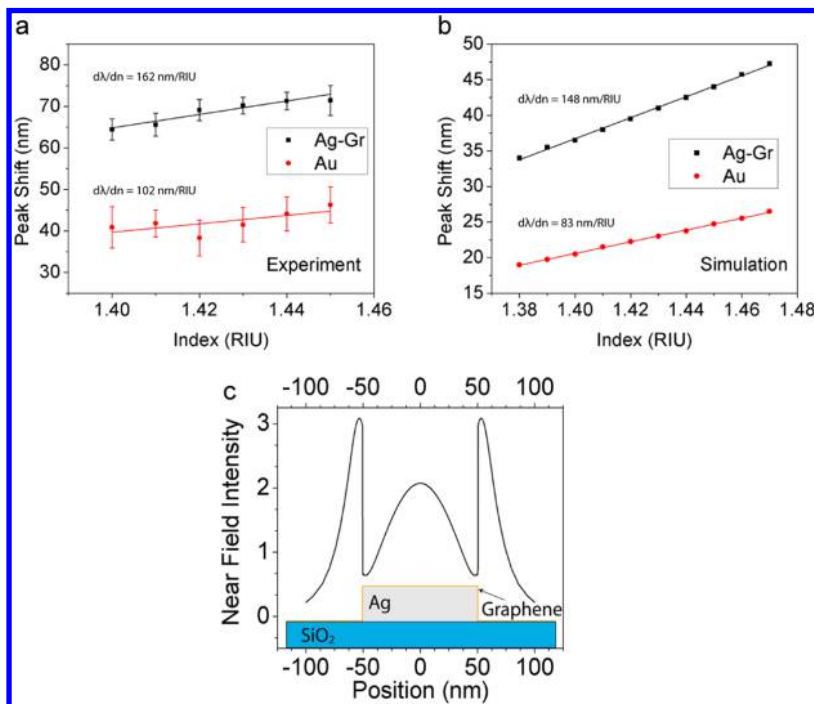


Figure 4. Sensitivity of both graphene-passivated silver as well as gold nanoantennas arrays of the same dimensions to bulk index changes over a small index range. (a) Experimental data for the change in peak wavelength with index, showing a bulk sensitivity ($d\lambda/dn$) of 162 for Ag–Gr and 102 for bare Au. Error bars represent one standard deviation over 20 individual, identical arrays. (b) Theoretical data from FDTD simulations showing a $d\lambda/dn$ of 148 for Ag–Gr and 83 for bare Au. (c) Plot of near field intensity profile from FDTD simulations of graphene-passivated silver nanoantennas as a function of position. The local enhancement of the electric field decays exponentially with a constant of 16.5 nm from the surface of the particle.

After the 30 day period, the graphene-passivated Ag showed a 2600% higher $dI/d\lambda$ over that of unpassivated silver (Supporting Information, Figure S4). Because of the impenetrability of graphene to sulfur species, it is believed that any degradation of the optical properties for graphene-passivated Ag nanoantennas is a result of imperfect graphene coverage of the nanoantennas across the $100 \times 100 \mu\text{m}^2$ array. Cracks in the graphene sheet cause a small fraction of the nanoantennas to remain unpassivated, leading to some degradation even in the graphene protected sample. The cracks resulting from the graphene transfer process account for approximately 2% of the graphene area (Supporting Information, Figure S5).

Raman spectroscopy was used to confirm the presence of graphene on the surface of the nanoantennas. Figure 3a shows the Raman spectra sampled on the Ag nanoantennas as well as on the substrate. Both spectra show the G- and 2D-bands with a higher intensity 2D band, suggesting monolayer graphene.²⁷ The wide peak around the G-band for the Raman signal on the

Ag nanoantennas comes from the fluorescence from the nanoantennas themselves. The data also shows about an order of magnitude enhancement in the Raman signal of the graphene when sampled on top of the nanoantennas in comparison to graphene just on glass. A Raman map highlighting the intensity of the 2D-band (Figure 3b) clearly shows the collective enhancement of the graphene Raman signal from the nanoantennas within the boundaries of the array.

One of the main concerns about protective layers on LSPR sensors is the detrimental effect it has on the sensitivity to local refractive index changes. Because graphene is only 0.355 nm thick,²⁸ it should not hinder LSPR sensing ability of the nanoantennas that is highly sensitive but also highly localized. For bulk refractive index sensing, similarly fabricated array samples were made that were 110 nm in diameter and 250 nm in interparticle spacing. To compare the Ag–Gr nanoantennas with that of Au nanoantennas, the second sample in this study was deposited with 3/30 nm Ti/Au in place of the Ag–Gr film.

These were then put into poly(dimethylsiloxane) (PDMS) fluid cells with refractive index matching liquids (Cargille, Series AA). The samples were washed with acetone/IPA and placed under vacuum for several hours between each refractive index liquid to ensure no residual chemical remained on the sample. Figure 4a shows the peak shift from air ($n = 1.00$) of both Ag–Gr and Au nanoantennas for a very fine and controlled refractive index range ($n = 1.40$ – 1.45), proving that graphene-passivated nanoantennas retain their ability to sense small local refractive index changes. The error bars signify one standard deviation in the peak position over 20 individual, identical $100 \times 100 \mu\text{m}^2$ arrays for each index. Measuring the resonance peak shift as a function of the index, the bulk sensitivity of the LSPR sensor from the slope of Figure 4a, $d\lambda/dn$, can be determined. For graphene-passivated Ag nanoantennas, $d\lambda/dn = 162 \text{ nm}/\text{RIU}$, while $d\lambda/dn = 102 \text{ nm}/\text{RIU}$ for Au nanoantennas. This yields $\sim 60\%$ increase in bulk sensitivity for Ag–Gr over that of bare Au nanoantennas. Using finite-difference time-domain (FDTD) calculations, the effect of bulk index changes on both Ag–Gr as well as bare gold nanoantennas was studied. FDTD simulations were done using a software package (Lumerical 7.5.4) on both Au and Ag–Gr plasmonic structures of similar dimensions as in the experimental case. Optical data for graphene was taken from work by Gray et al.,²⁹ while the data for Au and Ag was taken from Palik.³⁰ A plane wave source was introduced, and the reflected power flux as a function of frequency was measured for both cases with varying bulk index of the background ranging from 1.38 to 1.47 RIU. Additionally, the field intensity profile was taken across the middle of the 30 nm Ag–Gr simulation, showing the field enhancement. Figure 4b shows the results of the simulations; the sensitivity toward bulk index change is 148 for Ag–Gr and 83 for Au nanoantennas. The simulations give rise to $\sim 80\%$ increase in bulk sensitivity of Ag–Gr over that of Au.

For bulk sensitivity measurements, the results show that the graphene-passivated silver nanoantennas were better at sensing bulk index changes than bare gold nanoantennas. The experimental 60% increase matched well with the 80% increase of the FDTD simulations. Such a result was expected because of the better plasmonic properties of silver. This also matches previous work that numerically shows the same order of magnitude increase in sensitivity of graphene-passivated silver versus that of gold for surface plasmon resonance (SPR) sensing.³¹ The increased bulk sensitivity of Ag–Gr nanoantennas means that Ag–Gr can be used for sensors with a much higher resolution.

The FDTD simulations also show the local electric field enhancement around the Ag–Gr nanoantennas (Figure 4c), with the inset showing the corresponding size of the particle in the lateral direction. The field enhancement is about three times at the edge of the particle and decays exponentially with a decay constant of 16.5 nm for this system. This shows two things. One is that the graphene layer does not limit the sensing abilities of silver particles as the field still extends tens of nanometers from the surface. The second is that only a very thin and impermeable passivation layer is applicable in this system, such as monolayer graphene. Polymeric or ceramic passivation layers need to be on the order of hundreds⁹ or tens¹⁵ of nanometers in thickness, respectively. Given the fast decay of the localized field, such thick layers would hamper the sensing ability of the nanoantennas. The hexagonal structure of graphene and delocalized π -bonds can attract and adsorb various biomolecules,³² making graphene a potential adsorption

layer for molecular sensing.³³ Additionally, graphene can be converted to graphene oxide with a large number of surface functional groups that can be tailored to individual molecular sensing applications.^{34,35}

To find the theoretical effects of sulfidation, an extension of the quasistatic Mie theory known as the modified long wavelength approximation (MLWA) was used to incorporate the radiation damping and depolarization effects. For theoretical scattering data, a mathematical package (Mathematica 8) was used with calculations based on the MLWA, as reported by Kelly et al.³⁶ The far field scattering spectra of the theoretical Ag oblate spheroids when coated with varying thicknesses of Ag_2S were obtained through this method. Following established literature, it was assumed that the conversion of Ag into Ag_2S occurs uniformly with a conversion ratio of 1:1.6.⁹ The Ag_2S and Ag optical data were obtained from Bennett et al.³⁷ and Palik,³⁰ respectively. The size and geometry of the spheroids were chosen such that they best approximated the behavior and resonance wavelengths of the actual Ag discs used experimentally; here the minor axis was chosen to be 12.5 nm to have a 600 nm resonance peak. Figure 5a shows the calculated scattering intensities with an increasing

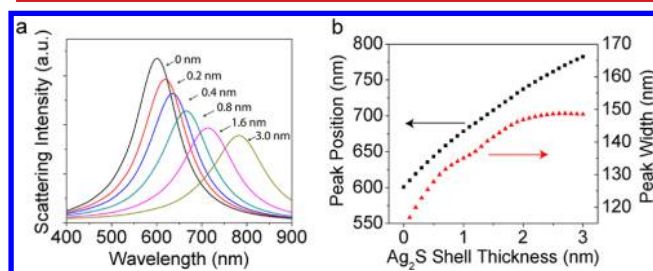


Figure 5. (a) Scattering intensity of Ag oblate spheroids with varying shell thickness of Ag_2S calculated with the MLWA. (b) Scattering peak position as well as peak width derived from the calculated scattering spectra.

uniform shell of Ag_2S around a Ag core in the spheroid. Both peak width and peak position as a function of Ag_2S shell thickness are shown in Figure 5b. Peak position increases roughly linearly with a slight plateau, whereas the peak width plateaus at a much faster rate.

From the theoretical scattering data, the general trend of increasing peak positions and line widths follows that of the aforementioned experimental data; however the rate at which it does so is different. This discrepancy can be explained by the morphological changes in the fabricated Ag nanoantennas. In Figure 2c, the resonance peak position for bare Ag nanoantennas increases at three different rates: a relatively steep rise, a plateau, and then another relatively steep rise. Based on the observations of Elechiquerra et al.,¹² the first steep rise in the LSPR peak position corresponds to a formation of silver sulfide crystallites around the Ag core. The larger index of Ag_2S causes the nanoantenna arrays to experience a red shift in the optical response, hence a steep rise in days 0–10. The plateau during days 10–14 corresponds to a period in which clusters of Ag_2S coalesce into a very rough shell of sulfide. The rough shell slowly grows and causes a relatively small red shift of the spectra but continue to increase the scattering loss, as seen in the increased peak width in Figure 2d. After day 14, the particles begin to break apart and fragment, leading to another large increase in the peak position. More significantly, the breaking up of the nanoantennas causes a substantial increase in

the peak widths. This splintering of the Ag nanoantenna is thought to be the result of changes in the crystal structure^{9,11} or through diffusive processes.¹⁴ It is believed that this is also the cause of the large increase in resonance peak width, even larger than that of theoretical values. Breaking of the nanoantennas would not only serve to enhance the rate of sulfidation but also dramatically increase scattering losses that lead to broadening of the optical spectrum. The morphological changes in the nanoantennas as a function of time can be seen in the Supporting Information, Figure S6.

In summary, by passivating the surface of Ag nanoantennas with graphene, we demonstrate that the sulfidation of the silver surface that degrades its excellent optical properties can be prevented by effectively blocking diffusion of gas molecules through a transferred monolayer graphene film. It is strongly believed that silver-based LSPR and SPR sensors and applications can now be significantly more useful, especially over long time frames without hindering near-field sensing. This method has the potential to be widely applicable to other plasmonic material systems otherwise rendered useless through chemical reactivity, such as Al or Cu nanoantennas. Not only are Al and Cu several orders of magnitude less expensive than gold, they both have different functional regimes for plasmonic sensors that can be enabled through graphene. Al is active in the deep-UV spectrum, while Cu is in near-IR. Thus, graphene passivation of metal nanoantennas has the potential to open up a wide range of plasmonic applications for reactive materials beyond silver alone.

■ ASSOCIATED CONTENT

Supporting Information

Supplemental Figures S1–S6. This material is available free of charge via the Internet at <http://pubs.acs.org>.

■ AUTHOR INFORMATION

Corresponding Author

*E-mail: cubukcu@seas.upenn.edu.

Notes

The authors declare no competing financial interest.

■ ACKNOWLEDGMENTS

This research was supported by startup funds from the University of Pennsylvania and partially by the Nano/Bio Interface Center through the National Science Foundation NSEC DMR08-32802.

■ REFERENCES

- (1) Jensen, T. R.; Malinsky, M. D.; Haynes, C. L.; Van Duyne, R. P. *J. Phys. Chem. B* **2000**, *104* (45), 10549–10556.
- (2) Xu, H.; Aizpurua, J.; Käll, M.; Apell, P. *Phys. Rev. E* **2000**, *62* (3), 4318–4324.
- (3) Haes, A. J.; Van Duyne, R. P. *J. Am. Chem. Soc.* **2002**, *124* (35), 10596–10604.
- (4) Hache, F.; Ricard, D.; Flytzanis, C. *J. Opt. Soc. Am. B* **1986**, *3* (12), 1647–1655.
- (5) Nie, S.; Emory, S. R. *Science* **1997**, *275* (5303), 1102–1106.
- (6) Pryce, I. M.; Kelaita, Y. A.; Aydin, K.; Atwater, H. A. *ACS Nano* **2011**, *5* (10), 8167–8174.
- (7) Adato, R.; Yanik, A. A.; Amsden, J. J.; Kaplan, D. L.; Omenetto, F. G.; Hong, M. K.; Erramilli, S.; Altug, H. *Proc. Natl. Acad. Sci.* **2009**, *106* (46), 19227–19232.
- (8) West, P. R.; Ishii, S.; Naik, G. V.; Emani, N. K.; Shalaev, V. M.; Boltasseva, A. *Laser Photonics Rev.* **2010**, *4* (6), 795–808.

(9) McMahon, M.; Lopez, R.; Meyer, H.; Feldman, L.; Haglund, R. *Appl. Phys. B: Lasers Opt.* **2005**, *80* (7), 915–921.

(10) Cao, W.; Elsayed-Ali, H. E. *Mater. Lett.* **2009**, *63* (26), 2263–2266.

(11) Huang, T.; Cao, W.; Elsayed-Ali, H. E.; Xu, X.-H. *Nanoscale* **2012**, *4* (2), 380–385.

(12) Elechiguerra, J. L.; Larios-Lopez, L.; Liu, C.; Garcia-Gutierrez, D.; Camacho-Bragado, A.; Yacamán, M. J. *Chem. Mater.* **2005**, *17* (24), 6042–6052.

(13) Nagpal, P.; Lindquist, N. C.; Oh, S.-H.; Norris, D. J. *Science* **2009**, *325* (5940), 594–597.

(14) Wang, L.; Xiong, W.; Nishijima, Y.; Yokota, Y.; Ueno, K.; Misawa, H.; Bi, G.; Qiu, J.-r. *Opt. Express* **2011**, *19* (11), 10640–10646.

(15) Park, Y.-i.; Cha, S.-w.; Saito, Y.; Prinz, F. B. *Thin Solid Films* **2005**, *476* (1), 168–173.

(16) Barrios, C. A.; Malkovskiy, A. V.; Kisliuk, A. M.; Sokolov, A. P.; Foster, M. D. *J. Phys. Chem. C* **2009**, *113* (19), 8158–8161.

(17) Hall, W. P.; Modica, J.; Anker, J.; Lin, Y.; Mrksich, M.; Van Duyne, R. P. *Nano Lett.* **2011**, *11* (3), 1098–1105.

(18) Geim, A. K.; Novoselov, K. S. *Nat. Mater.* **2007**, *6* (3), 183–191.

(19) Wang, X.; Ouyang, Y.; Li, X.; Wang, H.; Guo, J.; Dai, H. *Phys. Rev. Lett.* **2008**, *100* (20), 206803.

(20) Bunch, J. S.; van der Zande, A. M.; Verbridge, S. S.; Frank, I. W.; Tanenbaum, D. M.; Parpia, J. M.; Craighead, H. G.; McEuen, P. L. *Science* **2007**, *315* (5811), 490–493.

(21) Stoller, M. D.; Park, S.; Zhu, Y.; An, J.; Ruoff, R. S. *Nano Lett.* **2008**, *8* (10), 3498–3502.

(22) Kim, K. S.; Zhao, Y.; Jang, H.; Lee, S. Y.; Kim, J. M.; Kim, K. S.; Ahn, J.-H.; Kim, P.; Choi, J.-Y.; Hong, B. H. *Nature* **2009**, *457* (7230), 706–710.

(23) Leenaerts, O.; Partoens, B.; Peeters, F. M. *Appl. Phys. Lett.* **2008**, *93* (19), 193107–3.

(24) Bunch, J. S.; Verbridge, S. S.; Alden, J. S.; van der Zande, A. M.; Parpia, J. M.; Craighead, H. G.; McEuen, P. L. *Nano Lett.* **2008**, *8* (8), 2458–2462.

(25) Chen, S.; Wu, Q.; Mishra, C.; Kang, J.; Zhang, H.; Cho, K.; Cai, W.; Balandin, A. A.; Ruoff, R. S. *Nat. Mater.* **2012**, *11* (3), 203–207.

(26) Li, X.; Zhu, Y.; Cai, W.; Borysiak, M.; Han, B.; Chen, D.; Piner, R. D.; Colombo, L.; Ruoff, R. S. *Nano Lett.* **2009**, *9* (12), 4359–4363.

(27) Ni, Z. H.; Wang, H. M.; Kasim, J.; Fan, H. M.; Yu, T.; Wu, Y. H.; Feng, Y. P.; Shen, Z. X. *Nano Lett.* **2007**, *7* (9), 2758–2763.

(28) Gupta, A.; Chen, G.; Joshi, P.; Tadigadapa, S.; Eklund, P. C. *Nano Lett.* **2006**, *6* (12), 2667–2673.

(29) Gray, A.; Balooch, M.; Allegret, S.; De Gendt, S.; Wang, W.-E. *J. Appl. Phys.* **2008**, *104* (5), 053109–8.

(30) Palik, E. D. *Handbook of Optical Constants of Solids*; Academic Press: San Diego, 1985.

(31) Choi, S. H.; Kim, Y. L.; Byun, K. M. *Opt. Express* **2011**, *19* (2), 458–466.

(32) Song, B.; Li, D.; Qi, W.; Elstner, M.; Fan, C.; Fang, H. *ChemPhysChem* **2010**, *11* (3), 585–589.

(33) Papisimakis, N.; Luo, Z.; Shen, Z. X.; De Angelis, F.; Di Fabrizio, E.; Nikolaenko, A. E.; Zheludev, N. I. *Opt. Express* **2010**, *18* (8), 8353–8359.

(34) Han, T. H.; Huang, Y.-K.; Tan, A. T. L.; Dravid, V. P.; Huang, J. *J. Am. Chem. Soc.* **2011**, *133* (39), 15264–15267.

(35) Li, F.; Feng, Y.; Zhao, C.; Li, P.; Tang, B. *Chem. Commun.* **2012**, *48* (1), 127–129.

(36) Kelly, K. L.; Coronado, E.; Zhao, L. L.; Schatz, G. C. *J. Phys. Chem. B* **2002**, *107* (3), 668–677.

(37) Bennett, J. M.; Stanford, J. L.; Ashley, E. J. *J. Opt. Soc. Am.* **1970**, *60* (2), 224–231.